Int. Journ. of Wettability Science and Technology, Vol. 1, pp. 171–188
Reprints available directly from the publisher.
Photocopying permitted by license only.

Rapid Prototyping in the Application to the Dynamic Surface Tension Measurements

A. BALDYGIN[1,A], J. S. MARIN QUINTERO[1,A] , T. WILLERS[2] AND P. R. WAGHMARE[1,*]

[1]*Interfacial Science and Surface Engineering Lab (iSSELab), Department of Mechanical Engineering, University of Alberta, Edmonton, Alberta T6G2G8, Canada.*
[A]*The first two authors have contributed equally.*
[2]*KRUSS GmbH, Borsteler Chaussee 85, 22453 Hamburg, Germany.*

Traditional bubble tensiometers experience deviation of surface tension measurements at low surface ages – typically below two milliseconds. So, there is limited clarity on how the bubble formation process occurs and if there is any dependency on pipette geometry. In this paper different geometries of pipettes were designed, manufactured and evaluated for their affect in the growth of the bubbles while maintaining a constant air flow for each test. Two different shapes of tips were considered and verified; aspects changed were the outlet diameter, the length and the conical taper before the outlet. Consequently, pipettes were fabricated using additive manufacturing (3D printing), the bubble formation process was simulated and recorded with a high-speed camera, and finally the videos were analysed with a 2D image analysis software. In this context, the behaviour of the bubble growth changed according the geometry and the parameters of the pipette tip.

Keywords: CMC, DST, SFT, capillary, surface age

1 INTRODUCTION

Surface tension is one of the governing properties of the liquid phase that describes the propensity of a liquid to acquire the least surface area possible given its surroundings. In nature, we can observe that fluids, when they are suspended in a medium of a different phase, obtain a spherical shape caused

*Corresponding author: e-mail: waghmare@ualberta.ca

by the attraction of the molecules at the interface, tending to minimize the surface area [1]. Also, the surface tension can be defined as the work required to change the extent of the interfacial area of a phase. Nowadays in industry, there is a demand to optimize procedures to minimize operating times in different processes such as spraying, foaming, cleaning, printing, and coating [2].

Surface-active agents, conventionally known as surfactants, are utilized to reduce the surface tension and the energy required to produce new surfaces; as mentioned previously, the surface tension is one of the major factors that dictate the energy required to form the interface. When surfactant molecules are introduced, these surface active agents require a finite time to settle at the interface; changes in the surface tension during this time is based on the corresponding concentration of surfactants at the interface [3]. The quantification of this dynamic process is widely termed as the dynamic surface tension (DST) measurement, whereas the quantification of static surface tension is always measured once the interface is saturated with the available surface active agents [4]. Dynamic surface tension is an important parameter which allows characterizing a surfactants' diffusion and adsorption rate [5-9]. If the surface is completely covered or saturated with surfactant molecules, the remaining surfactant molecules within the bulk liquid phase start to aggregate and form micelles of different shapes [10]. At the point where these micelles start to form, the surfactant concentration is above the critical micelle concentration (CMC), and the surface tension becomes independent of concentration.

Different methods have been developed to measure both the dynamic and the static, or equilibrium, surface tension. To quantify the static surface tension, the Du-Noüy ring, the Wilhelmy plate, the spinning drop and the pendant drop methods are used [11]. For the dynamic surface tension, the bubble pressure and the drop volume method are the most common methods implemented. As mentioned earlier, the key difference for these measurements is the quantification of interfacial tension before attaining equilibrium or after attaining equilibrium. Here, we focus on the dynamic process of interface generation which plays a significant role in identifying the dynamic interfacial tension.

Bubble tensiometers are traditionally used to complete such measurements [6], [12-15]. It allows measurement of dynamic surface tension when the solution is primarily at or beyond the CMC. The bubble tensiometer uses the maximum bubble pressure method (MBPM) to obtain the surface age of the drop [16]. Dynamic surface tension is determined based on results for the maximum internal pressure measurements in a growing bubble or dilating bubble [13, 17-19].

The bubble pressure method typically uses a polypropylene or functionalized glass capillary submersed in a surrounding liquid media to produce gas bubbles and determine the surface tension of the liquid. Figure 1 shows the

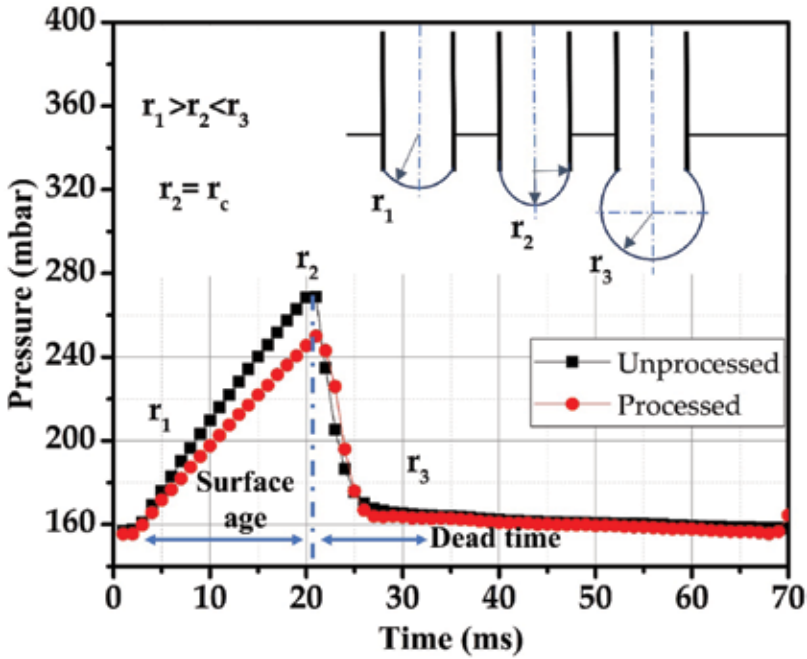

FIGURE 1
Pressure as a function of time in the bubble pressure method for water for two different capillaries. Processed capillaries are appropriately functionalized and machined to obtain the uniform interface generation whereas improperly-machined, unprocessed capillaries show lower pressures due to non-uniform generation of the interface. Schematics on the top right corner illustrate the radius growth at the tip of the capillary.

working principle of this method. The internal pressure of a spherical gas bubble (P) is a function of the instantaneous radius of curvature (r) and the surface tension (γ); with the Young-Laplace equation $\left(p = \frac{2\gamma}{r} \right)$ these variables can be correlated with each other [20]. The radii of the gas bubble attached to the tip of the capillary initially increases and then decreases, as seen in Figure 1. At the point where the curvature is the greatest, the maximum pressure is reached. At this moment, the radius of the curvature of the bubble is equal to the radius of the capillary, *i.e.*, $r=r_c$. The time from the start of the bubble formation to the occurrence of maximum pressure is called the surface age, and from the maximum pressure to the detachment of the bubble is called dead time. The measurement of the dynamic surface tension depends on the surface age; so, dynamic surface tension will vary according to the bubble production speed. Now, if the maximum pressure of the process (P_{max}) and the radius of the capillary (r_c) are known, and considering a correction factor for the hydrostatic pressure ($P_0 = \Delta\rho gH$) due to the immersion of the

capillary in the liquid, one can obtain the dynamic surface tension at a specific surface age [12, 17, 21] or the surface age with maximum surface tension as $\left(\gamma = \frac{\left(p_{max} - p_o\right) r_c}{2}\right)$.

Industrial processes are seeking opportunities to optimize processes and to reduce production time, *i.e.*, interaction time between objects and surface active agents [5, 7, 9, 12]. Thus, measurements need to be done at a relatively low time scale, *i.e.*, in the order of milliseconds for most cases [5, 13, 18, 22]. Special precautions are in place to take measurements below five milliseconds range, *e.g.*, at the millisecond interval [23]. The experimental data claims that the dynamic surface tension deviates from the expected numbers at the surface age in the range of milliseconds even for water measured at 20 °C [5, 13, 18, 22, 24]. The use of the damaged or aftermarket capillaries can lead to erroneous measurements in the pressure (as depicted in Figure 1, unprocessed capillary), resulting in false results in the dynamic surface tension or, even in some cases, higher or lower surface age [25]. In this paper, an attempt is made to study the process of the bubble formation concerning the geometrical configuration of the capillary. Different geometries and aspects of the capillaries are presented to comment on the preferable capillary tip configuration for the correct results. To pinpoint the necessity of such a study, dynamic surface tension measurements of widely used capillaries are presented using the bubble pressure method as seen in Figure 2. The results of surface tension deviate if an adequate capillary is not used proving there is an actual dependency on the capillary used and the surface tension measurement. Three different polymer capillaries, two with ideal surface finish (PPC2W and PPC3W) and one with a damaged end point (PPC1W), were used to measure the surface tension of water at room temperature, around 22 °C. The PPC nomenclature is used for polypropylene (PP) capillaries, whereas, W and S are for water and surfactant. PPC1W, PPC2W, PPC3W measured surface tension of water at 68.6 ± 3.2 mN/m, 72.5 ± 0.6 mN/m and 72.1 ± 0.4 mN/m, respectively; in comparison, the expected literature value for water is 72.45 mN/m. It can clearly be seen that PPC1W differs from expected nominal value, especially at a low surface age where bubble formation rapidly happens. In the case of bubble pressure tensiometry, the main motivation is the ability to obtain the dynamic surface tension or the surface tension at certain surface age. To demonstrate this we used additional two sets of data, where the same water-dish detergent solution was used twice for two different capillaries, PPC4S and PPC5S. One of them, PPC4S, has defects at the end point, which resulted in a significant overestimation of the surface tension in the range of 0-200 ms. An unprocessed capillary can also be attributed to the same deficiency. Thus, it is evident that the detail understanding of the role of the geometry of the capillary is necessary which is presented in the later section.

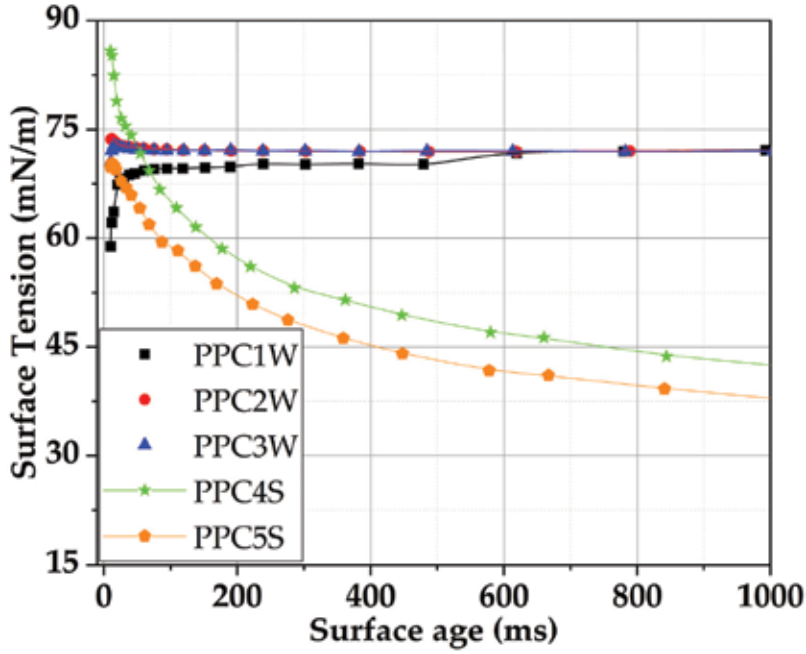

FIGURE 2
Variations in the surface tension measurements due to subtle differences in the tip geometry. Surface tension measurement of water as a function of surface age for three different polymer capillaries (PPC1W, PPC2W, PPC3W), and surface tension measurement of water-dish detergent solution as a function of surface age for two different polymer capillaries (PPC4S, PPC5S).

Another attempt is made to optimize parameters for the instrument components, involved in bubble pressure tensiometry, and to increase precision in the measurements carried out. It was found that narrow capillaries with a radius below 150 microns lead to optimum and reproducible results [12, 16, 18, 21, 26]. A dependency was recognized between the bubble growth and the volume of the separating bubble, the length and the radius of the capillary [8]. The importance of reliable data interpretation is described by Kovalchuk et al. [27], where some of the dynamic effects also depend on the geometry of the capillary. Thus, there is a need to perform studies where the inside and outside geometry of the pipette is taken into consideration.

2 MATERIALS AND METHODS

There are a few industry standard designs established for capillaries compatible with the bubble pressure tensiometer [13]. A variation of geometrical conical or cylindrical expansion of the inner and outer diameter of a capillary

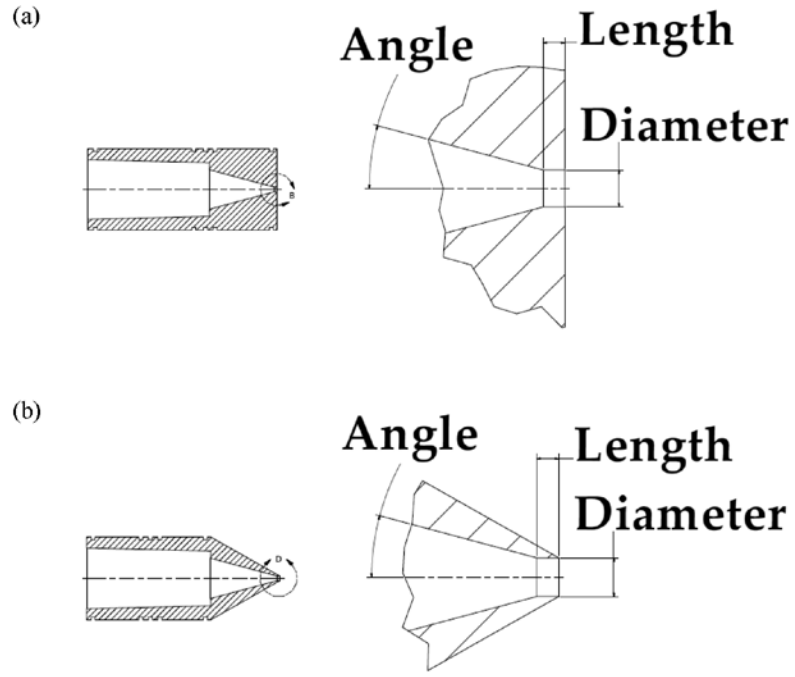

FIGURE 3
Established capillary design, where (a) Flat tip model and (b) Cone tip model.

can assure uniform gas bubble growth [23]. Based on provided examples, two different types of tips are designed as shown in Figure 3 where geometrical aspects such as the diameter, the length, and the angle of the capillary are varied. These capillaries are used to evaluate the behavior of the bubble formation process.

Currently, manufacturing cycles are shortened due to recent developments in advanced manufacturing and rapid prototyping [28-30]. These developments not only allow to produce the necessary accessories for the bubble pressure tensiometer directly onsite and minimize downtime but also enable rapid optimization of geometrical aspects of a capillary [31, 32]. Hence, in this study we adopted 3D printing technology to produce tip geometries for bubble pressure measurements.

Pipettes were fabricated with the use of the desktop stereolithography (SLA) 3D printer (Form 2, Formlabs Inc.) equipped with black resin (GPBK02, Formlabs Inc.). To enhance the quality of the holes at the tip of the pipette or capillary, a cleaning procedure was established. Due to the nature of the black resin, hydrophobic behavior is observed at the tip surface at the end of the manufacturing process and remained unchanged through the tests.

The Surface Free Energy (SFE) or polarity of the pipettes was not enhanced with either chemical, plasma or coronas treatment prior to each measurement. Software (PreForm, Formlabs Inc.) provided with the 3D printer was used to set model orientation at 45 ° Y-rotation with respect to the build platform with the open holes of the capillary facing downwards to allow resin drainage. The layer thickness was limited by the printer configuration and was set to 25 microns. To verify printed components, the diameter and circularity of the hole were measured with the fully automated inverted research microscope (DMI 6000 B, Leica Microsystems Inc.). The wettability of the tip of the pipette surface was quantified by measuring the contact angle with goniometer and it was observed that the tips are hydrophobic in nature presenting contact angle in the range of 90 to 100°. A nomenclature was created and used to differentiate configurations of the pipettes. It included the model, the trial number, the nominal diameter, and length of the hole. An example is shown in Figure 4. In the model component, 1 stands for a flat pipette and 2 represents a cone pipette, and all the measurements of the hole are presented in millimeters.

The generation of the bubble, or interface, with a bubble pressure tensiometer ranges from a millisecond to a few seconds, and to mimic this process a goniometer (DSA100E, KRÜSS Scientific Instruments Inc.) with ultra-flexible fiber-optic-arm lights (Part number 14815T41, McMaster-Carr Supply Co.) and high-speed camera (Phantom V711, Vision Research Inc.) is used as depicted in Figure 5. The single software-controlled syringe dispenser, installed on the goniometer, is used to generate the air bubbles in water media through the disposable syringe (NORM-JECT 1mL, Henke-Sass Wolf GmbH) with the capillary attached to it. During a single discharge process, several air bubbles were generated with the

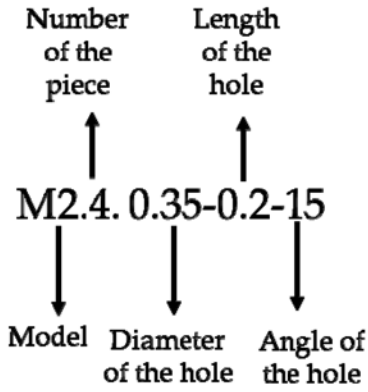

FIGURE 4
Example of the nomenclature used for the pipettes, which represents the fourth piece of a cone model with a diameter hole of 0.35 mm with a hole length of 0.2 mm with an angle of 15°.

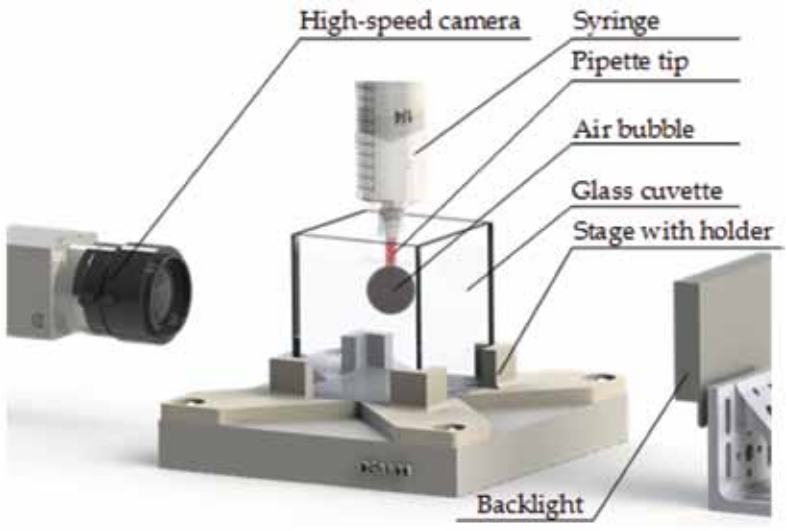

FIGURE 5
Artist impression of the configuration used to conduct the experiments.

total volumetric volume of 60 microliters at a low rate of 500 μL/min. The distortion-free glass cuvette (SC02, KRÜSS Scientific Instruments Inc.) prefilled with the distilled water (DI) produced from a water purification system (PURELAB© Ultra, Elga Labwater, LLC) is used to obtain the bubble growth. In addition to this, to compare the results obtained with the goniometer setup, experiments with a bubble pressure tensiometer (BP100, KRUSS Scientific Instruments Inc.) were also been carried out. The glass cuvette is placed on the stage and the backlight from the tensiometer is used to illuminate the bubble formation/growth process while the high-speed camera captures at 16,800 frames per second (fps). This measurement is used as a reference to compare the results with those of the rapid prototype capillaries. All measurements were performed at ambient conditions.

The proposed approach assumed the humidity of the surrounding air and the pH level of the water reservoir is constant. The change in pH level during the measurement is not significant hence it can be safely ignored. Literature suggests that the relative humidity of air in the range of 30-40% can be responsible to change the surface tension of water from 72.45 mN/m at 22 °C to a range of 76 to 76.5 mN/m [33]. However, in our opinion, the timescale at which the relative humidity affects the interfacial tension as opposed to the measurement time scale with bubble pressure are at different. Therefore, one can safely ignore the role of pH.

For measurements for 3D printed capillaries using the goniometer, the high-speed camera is controlled using master software (Phantom Camera Controlled (PCC), Vision Research Inc.) where the recording rate was set to 13,000 fps at a resolution of 800x600 pixels. Imaging settings, *i.e.*, exposure, focus, white inten-

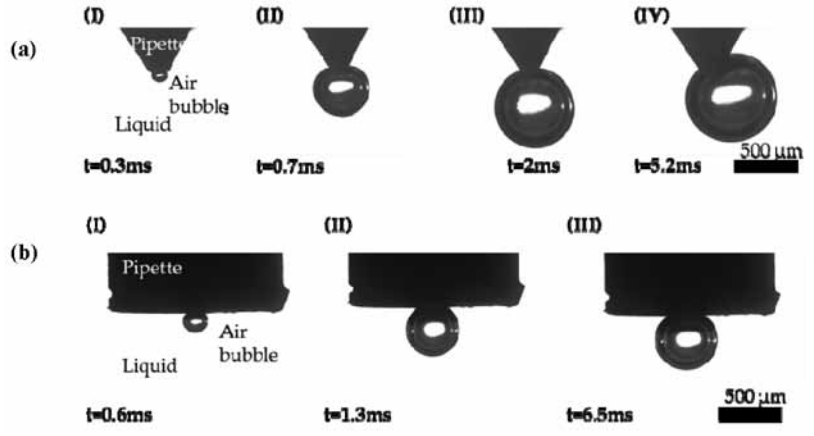

FIGURE 6
(a) Stages of the bubble growth using M2.4.0.35-0.2-15: (I) Initial growth of the bubble; (II) intermediate growth of the bubble; (III) final growth of the bubble; (IV) the detachment of the bubble. (b) Stages of the bubble growth process using M1.2.0.34-0.05-15: (I) initial growth of the bubble; (II) intermediate growth of the bubble; (III) final growth of the bubble.

sity and color balance, were set manually and optimized during the process. Captured videos were further processed and analyzed with the commercially available image analysis software (ImagePro Premier 9.2, Media Cybernetics, Inc.). Examples of bubble growth for two distinguishable outside configurations are shown for the cone and flat pipettes in Figure 6.

An example, shown in Figure 6 (a), demonstrates the different stages of a bubble growth process but for a cone pipette (M2.4.0.35-0.2-15). During the growth process, the bubble experiences three stages: the initial growth of the bubble Figure 6 (a)-I, where the mean diameter and circularity of the bubble are increasing with time. The intermediate growth of the bubble Figure 6 (a)-II, where the maximum circularity is reached, and the mean diameter is increasing with time. Moreover, the final growth of the bubble Figure 6 (a)-III, where the circularity is not constant with increasing diameter. An additional stage, *i.e.*, the detachment of the bubble in the case of Figure 6 (a)-IV is shown to identify the difference in the detachment of the bubble in the case of the conical pipette. Another example, shown in Figure 6 (b), demonstrates the different stages of a bubble growth process for a flat pipette M1.2.0.34-0.05-15. Similar to the previous pipette, the growth process goes through three stages.

As mentioned earlier, the geometry of printed pipettes was verified/measured with the use of a microscope. To statistically represent the success rate of a manufacturing process, a processing code was developed using a commercial multi-paradigm numerical computing environment (MATLAB R2017b MathWorks). This functionality allows to align centers of the open holes and to stack them into an averaged image, which represents the averaged geometry of a

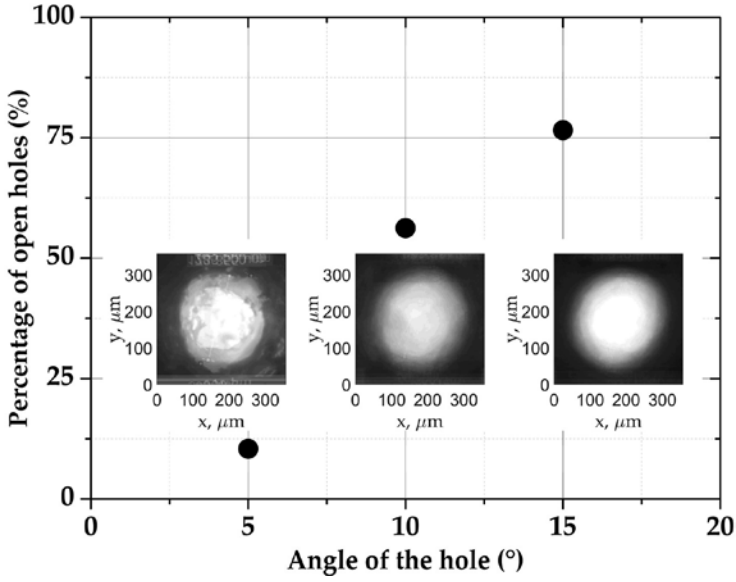

FIGURE 7
Percentage of clear aperture holes in different angles of the capillary.

selected configuration. It permits to understand the manufacturing success rate and optimize specific printing parameters to achieve the desired geometry. The algorithm is similar to the one used to find attractive faces where digitized photo samples were mathematically averaged [34-36].

3 RESULTS

In total, fifty-four (54) different configurations of pipettes were manufactured with diameters of 0.35, 0.34 and 0.32 mm, lengths of 0.05, 0.1 and 0.2 mm and angles of 5, 10 and 15° for each type – flat and cone tip. The list of these configurations can be found in the supplementary document in tabulated format. The final finish of the produced holes with the use of the desktop stereolithography (SLA) 3D printer was verified for the circularity and nominal diameter. The collected data for both tips, flat and cone, is shown in Figure 7, where the vertical axis represents the percentage of open holes and the horizontal axis is the angle of the cavity. One can speculate that to guarantee an open hole with a high circularity, a design of the capillary should have a higher inner cone angle around 15°.

The circularity, or roundness, is a dimensionless parameter that describes how close an object is to a true circle, and the mean diameter is the diameter that best defines this circle. By knowing how the circularity grows in time, the assumption

of a perfect sphere of a bubble can be tested during the measurements, where it is essential to define the gas-liquid interface accurately, which subsequently quantifies the interfacial property. The shape of the growing bubble can provide insights into the additional forces and effects that are usually negligible or ignored during such measurements. These forces are due to the viscous stress, drag caused by external media and surface tension gradient. Hence, the mean circularity of the bubble with its mean diameter quantification must be obtained to understand and delineate the role of these additional effects. Apart from the fluid dynamics aspect, which is system dependent, the pipette geometry or configuration, which is similar in all cases irrespective of the fluid medium, is another important parameter that governs the bubble growth. In this paper, analysis of bubble shape is performed during the dead time, see Figure 1 for reference. Future research of the bubble formation process during surface age time is needed to completely understand the process. Therefore, we categorically studied the role of each geometrical aspect of the pipette. As presented in Figure 3, the pipette geometry can be defined using three dimensions, namely, pipette tip diameter, length of the constant diameter section and the cone angle.

3.1 Role of pipette length on bubble generation

To study the role of the constant diameter section we varied the length of the hole into three representative lengths and two cases are studied for both, cone and flat tips, as shown in Figure 8. The cone model with sharp end at the tip of the pipette is presented in Figure 8 (a) whereas Figure 8 (b) depicts the similar study for the

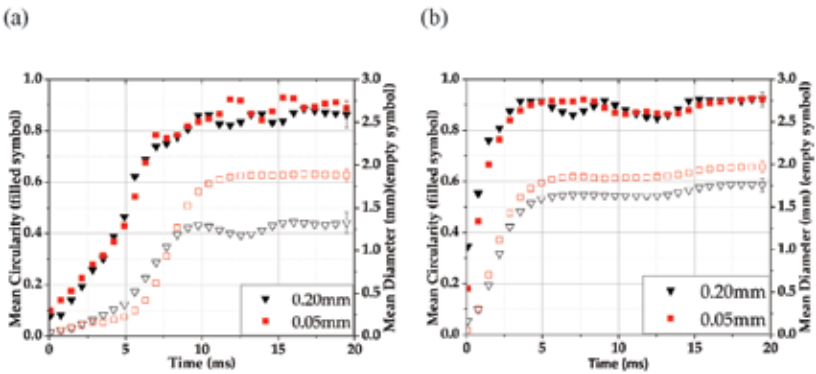

FIGURE 8
Comparison example of circularity and mean diameter of the growing air bubble in a liquid media for different hole lengths for (a) cone model and (b) flat model. Pipettes M2.2. 0.35-0.2-15 and M1.2. 0.35-0.2-15 are represented with black inverted triangles, and pipettes M2.1. 0.35-0.05-15 and M1.1. 0.35-0.05-15 are represented with red squares. Filled points represent the mean circularity of the bubble and empty symbols represent the mean diameter. Two capillaries with the hole diameter and angle of 0.35 mm and 15° are presented for both models with two different lengths of 0.05 and 0.2 mm. The error bar is the maximum deviation observed for all the measurements in that series.

flat end. The detailed investigations of the cone model suggest that the length of the constant diameter section has a role in defining the shape of the bubble. The filled symbol and the empty symbol in Figure 8 (a) represent the mean circularity and mean diameter, respectively. The inverted triangle and square are for the longer and shorter pipette, respectively. The growth rate of the bubble was approximately the same for both the cases, but, surprisingly, in the case of shorter length constant diameter hole the bubble oscillates after the maximum growth is achieved. The mean circularity was similar in both the cases, but the oscillatory behavior was noticed in the case of pipette with shorter length holes. On the other hand, the mean diameter was different for two different capillaries, which we can attribute to the frictional losses and loss of the energy due to the additional length of the holes. The pipette with smaller length hole (empty squares) attains the maximum mean diameter slower in the absence of oscillations and it remains contacts without any fluctuations. One can argue that in the cone model, the mean circularity does not change significantly as a function of the length of the hole.

In contrast to the cone model, for the flat capillary the small variation in the length does not play a significant role in defining the shape and growth of the bubble. The circularity grows at the same rate for both lengths and starts oscillating when the diameter reaches a maximum. The subtle difference is the frequency of oscillations in the mean circularity which can be investigated further with varied length pipettes. As mentioned earlier, the increase in the length reduces the size of the bubble in the cone tip but with the flat model this difference is smaller. Hence, the length of the hole is not the only reason for the difference in the mean diameter as witnessed in the cone model. But in the studied case, in Figure 8, the diameter of the tip or the pipette and the internal cone angle was constant. Hence, the external factors such as the static and dynamic pressure from the external liquid might be one of the prime reasons for this large deviation in the case of the cone model. It can be speculated that in the case of cone model, the moving interface has to displace the entire bulk liquid in circumferential direction whereas with the flat tip the primary displacement is only in one direction, *i.e.*, normal to the flat section of the pipette. The difference in the resistance experienced by the growing interface suggests that the flat tip is preferable to obtain the uniform growth insensitive to the length of the constant diameter section. In addition to the role of this geometrical parameter, it is worthwhile to study the impact of diameter and cone angle on the bubble growth which is presented in the subsequent sections.

3.2 Role of pipette diameter on bubble growth

To study the influence of the hole diameter on the bubble growth, we fixed the length and angle of the hole to 0.05 mm and 15° respectively. In the cone model as presented in Figure 9 (a), by maintaining the flow rate constant and increasing the hole diameter, the stream velocity will be reduced accordingly which will lead to a slower bubble growth. A bigger hole diameter will bring the possibility to grow a bubble with a larger diameter, but at a slower rate. This can be seen in the slope of the mean diameter curve for the 0.35 mm diameter as it is

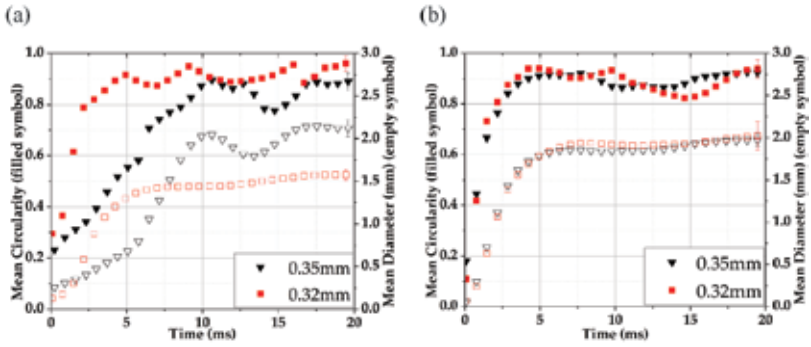

FIGURE 9
Comparison example of circularity and mean diameter of the growing air bubble in a liquid media for different opening diameters for (a) cone model and (b) flat model. Pipettes M2.2. 0.35-0.05-15 and M1.1. 0.35-0.05-15 are represented with black inverted triangles, and pipettes M2.4. 0.32-0.05-15 and M1.1. 0.32-0.05-15 are represented with red squares. Filled points represent the mean circularity of the bubble and empty symbols represent the mean diameter.

smaller and takes more time to reach its maximum value, which is higher compared to the 0.32 mm tip. The small difference in the tip diameter (0.03 mm) resulted in a 26% difference in the bubble diameter which is an interesting observation. Also, the oscillations in the circularity and mean diameter are more pronounced as diameter increases. We speculate that the larger diameter opening results in a non-uniform growth in a bubble and, in the attempt of minimizing the surface area as well as the surface energy, the bubble attempts to attain the spherical shape hence the oscillatory behaviour is observed.

However, the flat pipettes presented a different response (Figure 9 (b)) compared to the conical tip and the observation is similar to the previous section where the role of conical length section of the pipette is investigated. The flat model is again marginally sensitive to the changes in the geometry compared to the cone model. The slope, the oscillations, and maximum values of the diameters of the bubbles are relatively equal. As mentioned earlier, the growing interface in both the cases (with flat and conical tip) is different; in particular, with the flat tip the change in the pipette diameter does not hamper this resistance from the outside liquid medium. With the varied diameter case also, the circularity stops growing when the diameter reaches a maximum and thereafter the bubble oscillates until it detaches.

3.3 Role of pipette angle on bubble growth

To study the influence of the geometrical inner angle of the hole, refer to Figure 3, both types of capillaries, with a fixed diameter and length, change in cone angle from 10° to 15° and are studied for bubble growth. As suspected, the bubbles in the cone model are more sensitive to the change in the geometrical aspects, as depicted in Figure 10 (a). The greater angles result in

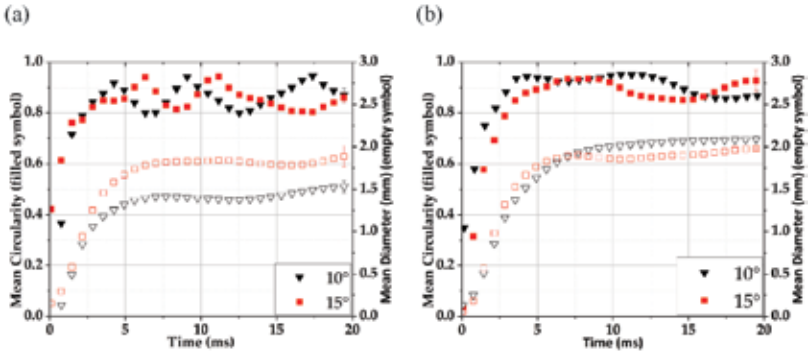

FIGURE 10
Comparison example of circularity and mean diameter of the growing air bubble in a liquid media for different hole angles for (a) cone model and (b) flat model. Pipettes M2.4. 0.35-0.05-10 and M1.3. 0.35-0.1-10 are represented with black inverted triangles, and pipettes M2.3. 0.35-0.05-15 and M1.1. 0.35-0.1-15 are represented with red squares. Filled points represent the mean circularity of the bubble and empty symbols represent the mean diameter.

larger area hence the observation was similar to the increase in the diameter but the growth was steady and similar to each other. With increased angle one can obtain a larger bubble with the same growth rate. Hence, for a conical tip, it can be concluded that increasing the angle is a better option as opposed to increasing the diameter in order to obtain a larger surface area bubble. More importantly, the oscillatory behavior is in phase and in the case of changing the diameter the difference in the oscillations was significantly different. This suggests that the drop oscillations are more sensitive towards the tip diameter. Thus, for conical tips, bubbles will grow at an equal rate for varied cone angle, with the only difference being that the tips with higher angles will generate larger bubble and it will require more time to achieve a stable bubble diameter. In the case of the flat tip, there is no relevant differences in the bubble growth as seen in Figure 10 (b). In both types of pipette, the drop oscillations are evident after the achievement of maximum diameter. With this parametric study, it is certain that the flat tip is the appropriate geometry for bubble growth.

3.4 Validation test

Finally, it is crucially important to compare and validate the growth of the bubble with widely used pipettes in bubble pressure tensiometry, *i.e.*, glass pipette. Therefore, we selected the best performing pipettes from cone and flat model and compared the bubble growth by these pipettes with the bubble grown with a bubble pressure tensiometer with attached glass pipette. Figure 11 demonstrates the comparative analysis and it is clearly evident that the flat capillary manufactured with the help of 3D printing technology demonstrated

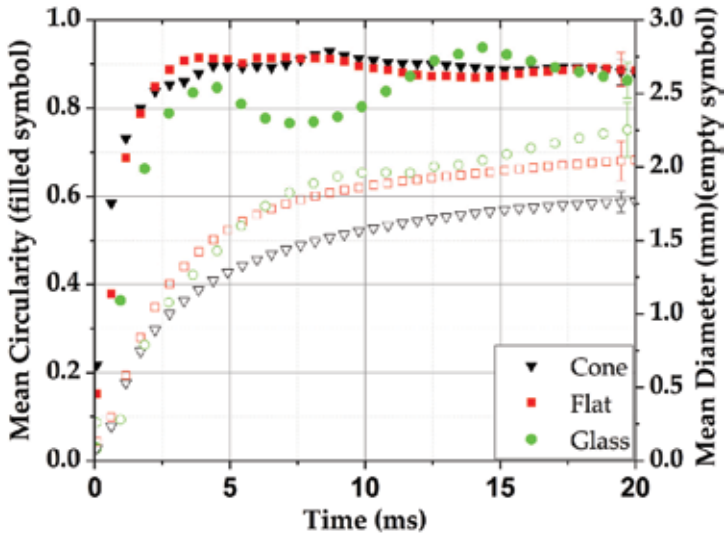

FIGURE 11
Example of the experimental results for the cone and flat model of the circularity and the mean diameter of the bubble, with a configuration of 0.35 mm diameter, 0.2 mm length of the hole and 15 ° inclination.

promising behavior. If the oscillatory nature of the expanding or the completely grown bubble is observed, then surprisingly the cone geometry pipette outperformed the glass pipette when bubble growth is recorded during the dead time. After scrutinizing the results further, it can be found that the cone model gives a difference of ± 0.029 and ± 0.070 mm for the circularity and mean diameter of the bubble, respectively. On the other hand, the flat model presents ± 0.038 and ± 0.134 mm of variations in the circularity and mean diameter of the bubble (respectively) by circumventing the oscillatory growth in the bubble. In addition to it, the flat pipette produces bubbles with the more extensive mean diameter while circularity remains the same as for the cone model.

4 CONCLUSIONS

From the comparative analysis, it is evident that rapid prototyping technology can be utilized in manufacturing pipettes for Bubble Pressure Tensiometry (BPT) and can be a replacement to traditional manufacturing processes. Printed cone and flat tip capillaries demonstrated promising dynamics during bubble formation process. The flat pipette produces bubbles with more extensive mean diameter while circularity remains the same as for the cone model.

The difference in the resistance experienced by the growing interface suggests that the flat tip is preferable to obtain uniform growth that is insensitive to the length of the constant diameter section. The growing interface in both the cases (with flat and conical tip) is different; in particular, with the flat tip the change in the pipette diameter does not hamper resistance from the outside liquid medium. In both types of pipette, drop oscillations are evident after the achievement of maximum diameter. With this parametric study, it can be supposed that the flat tip is the appropriate geometry for the overall bubble growth.

5 ACKNOWLEDGMENTS

The Authors are thankful to Dallyn Wynnychuk and Iman Roy for patent search and with measurements with the glass pipette. Authors are also thankful to Raymond Sanedrin, Selina André, and Carsten Gerber for their contribution to this work at various stages. In addition, authors are greatly thankful to Ryan Baily for assisting in improving readability, structure and organization of the paper. This research was partially funded by Natural Sciences and Engineering Research Council (NSERC) grant number RGPIN-2015-06542.

REFERENCES

[1] Bormashenko E.Y., *Wetting of Real Surfaces*, Berlin: De Gruyter. 2017.
[2] Muller N., Kinetics of micelle dissociation by temperature-jump techniques. Reinterpretation, *Journal of Physical Chemistry* **76** (1972) 3017–3020.
[3] Butt H.J., Graf K. and Kappl M., *Physics and Chemistry of Interfaces Third Edition*, Weinheim: Wiley-VCH. 2013.
[4] Holmberg K., Bo J., Kronberg B. and Lindman B., *Surfactants and Polymers in Aqueous Solution,* Chichester: John Wilety & Sons Ltd. 2003.
[5] Fainerman V.B., The maximum bubble pressure tensiometry, *Studies in Interface Science* **6** (1998) 279–326, 1998.
[6] Christov N.C., Danov K.D., Kralchevsky P.A., Ananthapadmanabhan K.P. and Lips A., Maximum bubble pressure method: Universal surface age and transport mechanisms in surfactant solutions, *Langmuir* **22** (2006) 7528–7542.
[7] Daniel R.C. and Berg J.C., A simplified method for predicting the dynamic surface tension of concentrated surfactant solutions, *Journal of Colloid and Interface Science* **260** (2003) 244–249.
[8] Mishchuk N.A., Fainerman V.B., Kovalchuk V.I., Miller R., and Dukhin S.S., Studies of concentrated surfactant solutions using the maximum bubble pressure method, *Colloids and Surfaces A: Physicochemical and Engineering Aspects* **175** (2000) 207–216.
[9] Chang C.H. and Franses E.I., Adsorption dynamics of surfactants at the air/water interface: a critical review of mathematical models, data, and mechanisms, *Colloids and Surfaces A: Physicochemical and Engineering Aspects* **100** (1995) 1–45.
[10] Tanford C., Micelle shape and size, *Journal of Physical Chemistry* **76** (1972) 3020–3024.
[11] Hiemenz P.C. and Rajagopalan, *Principles of Colloid and Surface Chemistry Third Edition,* New York, NY: Marcel Dekker Inc. 1997.

[12] Fainerman V.B. and Miller R., Maximum bubble pressure tensiometry - An analysis of experimental constraints, *Advances in Colloid and Interface Science* **108–109** (2004) 287–301.

[13] Fainerman V.B., Kazakov V.N., Lylyk S.V., Makievski A.V. and Miller R., Dynamic surface tension measurements of surfactant solutions using the maximum bubble pressure method – limits of applicability, *Colloids and Surfaces A: Physicochemical and Engineering Aspects* **250** (2004) 97–102.

[14] Lylyk S., Makievski A.V., Koval'chuk V.I., Schano K.-H., Fainerman V.B. and Miller R., The effect of capillary characteristics on the results of dynamic surface tension measurements using the maximum bubble pressure method, *Colloids and Surfaces A: Physicochemical and Engineering Aspects* **135** (1998) 27-40.

[15] Dixit N., Zeng D.L., and Kalonia D.S., Application of maximum bubble pressure surface tensiometer to study protein-surfactant interactions, *International Journal of Pharmaceutics* **439** (2012) 317–323.

[16] Fainerman V.B., Makievski A.V. and Miller R., Accurate analysis of the bubble formation process in maximum bubble pressure tensiometry, *Review of Scientific. Instruments* **75** (2004) 213–221.

[17] Bendure R.L., Dynamic surface tension determination with the maximum bubble pressure method, *Journal of Colloid and Interface Science* **35** (1971) 238–248.

[18] Dukhin S.S., Fainerman V.B., and Miller R., Hydrodynamic processes in dynamic bubble pressure experiments 1. A general analysis, *Colloids Surfaces A: Physicochemical and Engineering Aspects* **114** (1996) 61–73.

[19] Fukuta M., Sumiyama J., Motozawa M., and Yanagisawa T., Surface tension measurement of oil/refrigerant mixture by maximum bubble pressure method, *International Journal of Refrigeration* **73** (2017) 125–133.

[20] Mysels K.J., The maximum bubble pressure method of measuring surface tension, revisited, *Colloids and Surfaces* **43** (1990) 241–262

[21] Garrett P.R. and Ward D.R., A reexamination of the measurement of dynamic surface tensions using the maximum bubble pressure method, *Journal of Colloid and Interface Science* **132** (1989) 475–490.

[22] Austin M., Bright B.B. and Simpson E.A., The measurement of the dynamic surface tension of manoxol OT solutions for freshly formed surfaces, *Journal of Colloid and Interface Scence* **23** (1967) 108–112.

[23] Gertis E. J. M. and Perre W. V. D., Apparatus for Measuring Surface Tension. United States of America Patent 5,661,234, 26th August 1997.

[24] Dukhin S.S., Mishchuk N.A., Fainerman V.B., and Miller R., Hydrodynamic processes in dynamic bubble pressure experiments: 2. Slow meniscus oscillations, *Colloids and Surfaces A: Physicochemical and Engineering Aspects* **138** (1998) 51–63.

[25] Olson N.A., Synovec R.E., Bond W.B., Alloway D.M., and Skogerboe K.J., Dynamic surface tension and adhesion detection for the rapid analysis of surfactants in flowing aqueous liquids, *Analytical Chemistry* **69** (1997) 3496–3505.

[26] Fainerman V.B., Mys V.D., Makievski A.V., and Miller R., Application of the maximum bubble pressure technique for dynamic surface tension studies of surfactant solutions using the Sugden two-capillary method, *Journal of Colloid and Interface Science* 304 (2006) 222–225.

[27] Kovalchuk V.I. and Dukhin S.S., Dynamic effects in maximum bubble pressure experiments, *Colloids Surfaces A: Physicochemical and Engineering Aspects* **192** (2001) 131–155.

[28] Campbell T., Williams C., Ivanova O. and Garrett B., Could 3D Printing change the world? Technologies, potential, and Implications of Additive manufacturing, *Atlantic Council Strategic Foresight Initiative*, 2011 pp. 1–7.

[29] Mostafa, K., Qureshi A.J. and Montemagno C., Tolerance control using subvoxel grayscale DLP 3D printing, ASME 2017 International Mechanical Engineering Congress and Exposition, Tampa, Florida, USA, 2018, pp. 1–7.

[30] Weller C., Kleer R., and Piller F.T., Economic implications of 3D printing: Market structure models in light of additive manufacturing revisited, *International Journal of Production Economics* **164** (2015) 43–56.

[31] Duffy D.C., McDonald J.C., Schueller O.J.A., and Whitesides G.M., Rapid prototyping of microfluidic systems in poly(dimethylsiloxane), *Analytical Chemistry* **70** (1998) 4974–4984.

[32] Caprini D., Nascetti A., Petrucci G., Caputo D., and De Cesare G., Rapid prototyping of glass microfluidic chips based on autonomous capillary networks for physiological solutions, *18th AISEM Annual Conference, Trento, Italy, 2015* pp. 1–4.

[33] Pérez-Díaz J.L., Álvarez-Valenzuela M.A., and García-Prada J.C., The effect of the partial pressure of water vapor on the surface tension of the liquid water-air interface, *Journal of Colloid Interface Science* **381** (2012) 180–182.

[34] Langlois J.H. and Roggman L.A., Attractive faces are only average, *Psychological Science* **1** (1990) 115–121.

[35] Rhodes G., Geddes K., Jeffery L., Dziurawiec S., and Clark A., Are average and symmetric faces attractive to infants? Discrimination and looking preferences," *Perception* **31** (2002) 315–321.

[36] Langlois J.H., Roggman L.A., and Musselman L., What is average and what is not average about attractive faces?, *Psychological Science* **5** (1994) 214–220.